An alternative to the determination of the effective zero point in instrumented indentation: use of the slope of the indentation curve at indentation load values

Philippe Brammer, Olivier Bartier, Xavier Hernot, Gerard Mauvoisin, Simon-Serge Sablin

An alternative to the determination of the effective zero point in instrumented indentation: use of the slope of the indentation curve at indentation load values

P. Brammer[1,2,] , O. Bartier[1] , X. Hernot[1], G. Mauvoisin[1], and S.-S. Sablin[2]*

[1]LGCGM, Université de Rennes 1, 35042 Rennes Cedex, France

[2]Technocentre Renault, Vehicule Engineering – Material Engineering Department, 1 avenue du Golf, 78288 Guyancourt cedex, France

[*]Corresponding author: philippe.brammer@univ-rennes1.fr

Abstract

Most identification models based on instrumented indentation rely on the knowledge of the indentation load-penetration depth curve corresponding to the bulk material. Experimentally, and especially in the case of micro and nanoindentation testing, the measured curve can be affected by low scale artefacts such as sensor sensitivity, surface roughness, imperfect indenter tip geometry and material heterogeneity, leading to incorrect identifications of the indented material's bulk mechanical properties. This work proposes an exploitation of identification models which is based on the slope of the indentation curve at indentation load values and provides accurate results which are not affected by low scale artefacts.

1. Introduction

The indentation test data is obtained by continuously measuring the applied load F and penetration depth h of a stiff indenter of known geometry normally to the surface of the tested sample. The adequate exploitation of the data through reverse analysis leads to an evaluation of the indented material's mechanical properties. For the sake of simplicity, many reverse analysis models proposed in indentation literature **[1-12]** make the assumption that the sample is an homogeneous infinite half space, that the indented material obeys isotropic linear elastic behaviour, that its plastic yielding is predicted by the Von Mises yield criterion, its plastic behaviour is isotropic, and its isotropic hardening is described by the Hollomon power law, expressed by **Eq.1**.

$$\begin{aligned} \sigma &= E\varepsilon \quad (Hooke) \quad if \quad \varepsilon < \sigma_y / E \\ \sigma &= E^n \sigma_y^{1-n} \varepsilon^n \quad (Hollomon) \quad if \quad \varepsilon \geq \sigma_y / E \end{aligned} \qquad \textbf{(Eq.1)}$$

where σ is the true stress, ε the true strain, E the Young modulus, σ_y the yield stress and n the hardening coefficient.

Following these assumptions, reverse analysis, or identification models are created through intensive numerical simulating and data analysing, leading to proposals of explicit relations between experimental configuration, measured values, and material properties. In the case of an indentation by a rigid sphere, the general dimensionless form of this relation is given by **Eq.2**.

$$\frac{F}{E^* R^2} = \mathbf{\Pi}\left(\frac{h}{R}, \frac{\sigma_y}{E^*}, n\right) \qquad \textbf{(Eq.2)}$$

where R is the radius of the sphere and E^* the reduced elastic modulus given by **Eq.3**.

$$E^* = \frac{E}{1-\upsilon^2} \qquad \textbf{(Eq.3)}$$

where υ is the Poisson ratio of the indented material. The comparison of **Eq.2** with experimental results leads to the identification of the σ_y/E^* and n values which generate the smallest difference between the curve obtained from the model and the curve obtained experimentally. These values provide a stress-strain curve, described by the Hollomon law, which is frequently compared to the stress-strain curve obtained by a tensile test in order to assess the relevance of the material's mechanical behaviour evaluation.

The main advantages of the indentation test compared to the tensile test are the local probing of mechanical properties and the few restrictions on the sample shape and size. However, a drawback of the indentation test, if the objective is to identify bulk material properties, is its sensitivity to low scale artefacts such as sensor sensitivity, surface roughness, imperfect indenter geometry, and material heterogeneity **[13-19]**. These artefacts, independently from the assumptions on the bulk material behaviour, lead to deviations from the ideal *F-h* curve predicted by the identification models based on **Eq.2**.

Surface roughness cannot be completely eliminated during the preparation of the experimental samples, especially in the case of micro and nanoindentation, and the persisting asperities' height can be significant compared to the indenter radius and penetration depth. Initial contact between the indenter and the sample occurs on the asperities' peaks, and the slope of the *F-h* curve can be considered representative of the bulk material only once the asperities are compressed. However, if initial contact, i.e. zero penetration depth, is detected by the indentation device by a sharp rise of load **[15, 19]**, the penetration depth for a given load will show an offset $h_{offset,R}$ from the penetration depth measured in the case of a perfectly

smooth surface, corresponding to the compression of the asperities **[7, 14]**, such as presented schematically in **Fig.1**. Moreover, this offset as well as the necessary load for the compression of asperities is dependent on material properties, surface roughness, and the point of initial contact, i.e. the position of the indenter compared to the asperities' peaks and valleys **[14]**, which makes the determination of the effect of surface roughness impossible *a priori*.

Imperfect indenter geometry also has an effect on the *F-h* curve, such as in the case of cones with a blunted tip **[19]**. Indeed, in that case, the contact behaviour is initially that obtained with a spherical indenter, followed by a mix of that obtained with a spherical indenter and a conical one, until the conical geometry of the indenter dominates the evolution of the contact behaviour in which case the slope of the *F-h* curve can be considered representative of an indentation with a perfect cone. However, the bluntness of the tip results in an offset of the penetration depth $h_{offset,I}$ in comparison with the penetration depth obtained with an ideal cone, due to the incorrect tip position, and the slope of the *F-h* curve in the spherical and spherical-conical phases is obviously different from that obtained with an ideal cone, leading to the indentation curve represented schematically in **Fig.1**.

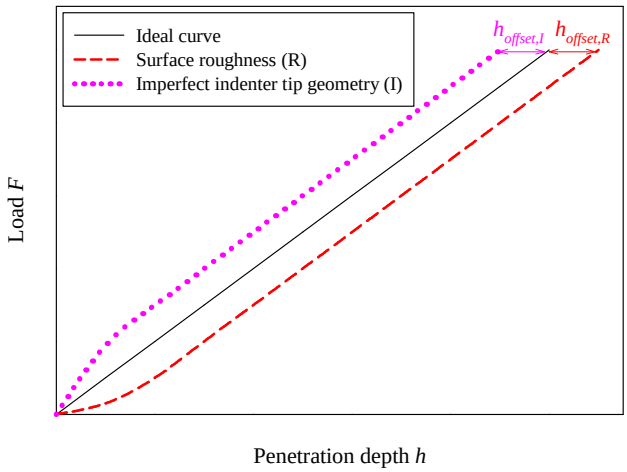

Fig.1. Effect of low scale artefacts on the indentation curve

Material heterogeneity can also affect the *F-h* curve. Indeed, it can be assumed that the slope of the *F-h* curve becomes representative of the bulk material behaviour only once the volume of material which is deformed is sufficiently large to be representative of a homogeneous material, leading to similar effects as those of surface roughness and indenter tip geometry imperfection.

An approach to overcome these effects is to redefine the effective zero penetration depth point and the *F-h* curve at low load values by extrapolating the indentation curve below a given non zero reference load **[13, 15, 19]**. However, this method presents inherent incertitude linked to the choice of the adequate reference load, extrapolation function, and fitting range **[13, 15]**, which are also unknown *a priori*. Other methods **[16-18]**, based on the use of a spherical indenter, rely on the availability of substantial initial elastic contact data and define the effective zero point and the *F-h* curve at low load values by fitting the initial results to the predictions of Hertz's theory **[20]**. This approach is generally not relevant if the determination of mechanical properties uses the *F-h* curve (i.e. models based on **Eq.2**) since plasticity occurs at very shallow penetration depth for most engineering materials.

The classical exploitation of identification models described by **Eq.2 [1-12]** to identify mechanical properties requires the knowledge of the *F-h* curve corresponding to the bulk material, i.e. presenting no offset of penetration depth nor effects on its slope at low load values, therefore the effects of the low scale artefacts described above, individually as well as coupled, can lead to wrong identification results, and the methods mentioned above may not be appropriate to overcome these effects. Therefore, there is an interest in proposing an exploitation of identification models based on **Eq.2** which is independent of the low scale artefacts mentioned above.

This work proposes such an approach based on the derivative of the *F-h* function instead of the *F-h* function itself. This approach does not require the determination of the effective zero penetration point and the perturbation of the slope of the *F-h* curve at low load values can be neglected. In section **2**, an identification model based on spherical indentation is chosen in the scientific literature, and its efficiency and its correct implementation are validated through comparison with finite element method (FEM) simulation. In section **3**, the effect of an offset of the penetration depth measurement on identification results is investigated, leading to an obvious requirement of an alternative approach. In section **4**, the alternative approach is proposed, and provides identification results which are little different from those obtained in the ideal case, whether the penetration depth or the slope of the *F-h* curve at low load values be different of the bulk material behaviour. In section **5**, an experimental case of an altered indenter tip is presented, showing effects on both the penetration depth and the slope of the *F-h* curve at low load values, eventually validating the approach proposed in this article.

2. Validation of the implementation of an existing identification model

Due to its simplicity of implementation, the identification model proposed in 2009 by Ogasawara et al. **[11]** is used. This model is defined for the indentation of an infinite half-space by a rigid sphere of radius R down to a maximal dimensionless penetration depth $(h/R)_{max}$=0.3. The indented material is assumed to obey isotropic linear elastic behaviour with a Poisson's ratio υ of 0.3. The yield criterion is Von Mises, the plastic behaviour is assumed isotropic, and the isotropic hardening curve is described by the Hollomon power law (**Eq.1**). The model is established using the Coulomb's friction law, with a friction coefficient μ=0.15. The material parameter domain covers a range larger than 1.67E-4 to 0.33 for σ_y/E^* and a range of 0 to 0.5 for n.

Spherical indentation simulations are carried out with the ABAQUS/Standard commercial finite element method code, in axisymmetric mode. All of the 10.000 mesh elements are axisymmetric four-node fully integrated elements. The element density distribution is built in order to obtain a compromise between accuracy in the contact and plastic zones, and computing time, as shown in **Fig.2**.

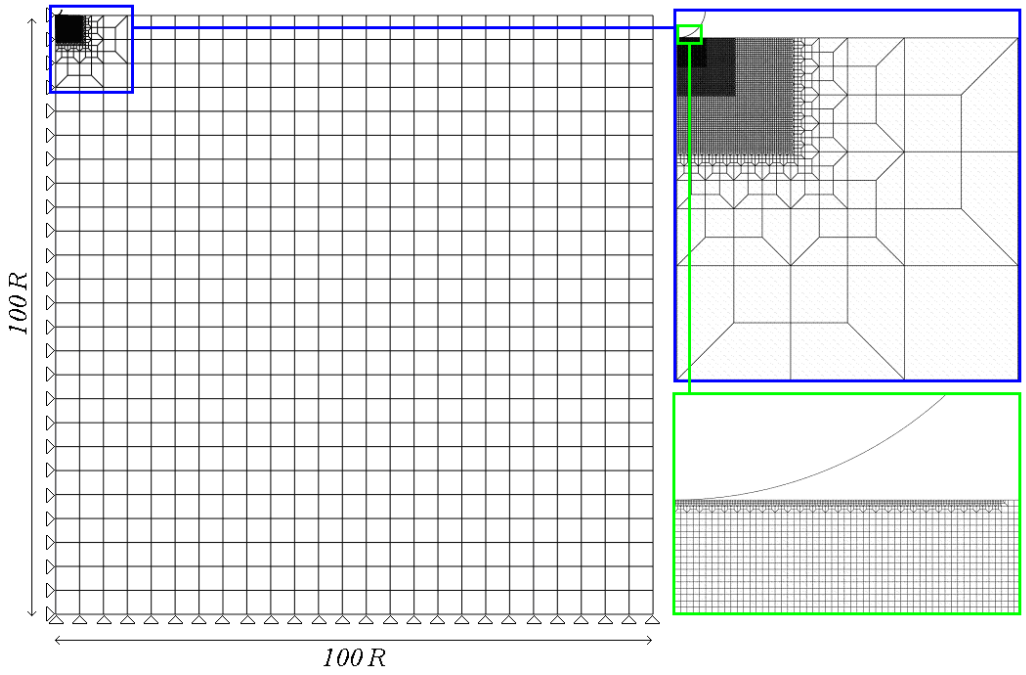

Fig.2. Mesh used for the simulation of spherical indentation

The friction coefficient for the penalty contact algorithm and the material's elastoplastic properties used in the FEM simulations are chosen in adequacy with the conditions of the model proposed by Ogasawara et al. (μ=0.15, υ=0.3). The Young modulus is set to a fixed value of 210 GPa, which is an average value measured on steel, and the yield stress (i.e. the σ_y/E^* ratio) and the hardening coefficient are varied. The six sets of material parameter values used for the simulations, which cover many classical engineering materials, are presented in **Table 1**.

	σ_y *(MPa)*	*n*
MAT 1	200	0.000
MAT 2	200	0.200
MAT 3	600	0.000
MAT 4	600	0.200
MAT 5	1000	0.000
MAT 6	1000	0.200

Table 1. Material parameter values used for the FEM simulations

The corresponding σ_y/E^* values are between 9.52E-4 and 4.76E-3, values which are contained within the definition range of the Ogasawara et al. model. The comparison and relative load difference between the indentation curves obtained from the model proposed by Ogasawara et al. and those obtained from the FEM simulations are presented in **Fig.3**.

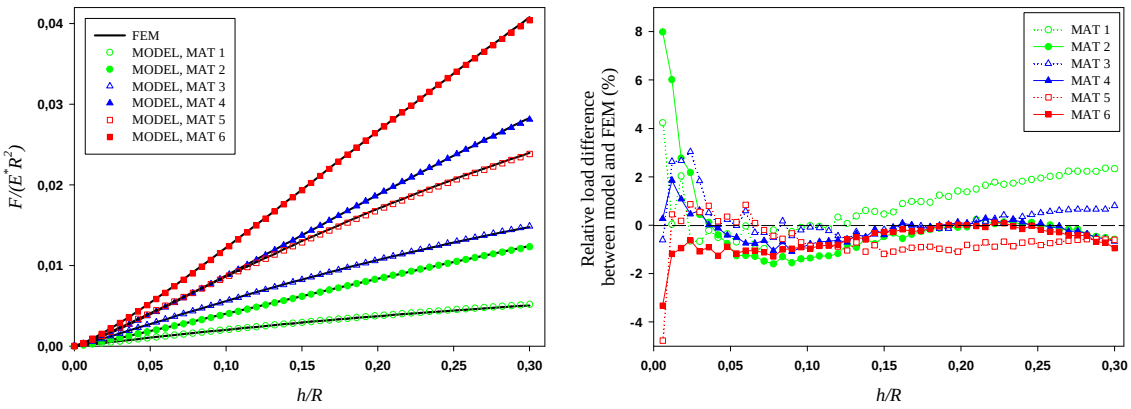

(a) **(b)**

Fig.3. (a) Comparison and **(b)** relative load difference between the indentation curves obtained from the model proposed by Ogasawara et al. and those obtained from the FEM simulations

Apart from the values at low penetration depth values where numerical particularities and/or model imperfections can generate noticeable differences, results show a very good agreement between the model proposed by Ogasawara et al. and the FEM simulations carried out in this work. Indeed, most error values are within the +/- 1% range.

The model proposed by Ogasawara et al. is then used to identify material parameter values from the FEM indentation curves which are taken as experimental data. The procedure proposed by Ogasawara et al. uses two data points of the experimental indentation curve at any two dimensionless penetration depth values between h/R=0.1 and h/R=0.3 to determine the two unknown parameters σ_y/E^* and n, however in this work the difference between the curve obtained from the model and the experimental curve is minimized over the whole penetration depth data, i.e. at all penetration depth values, using the classical least square based functional ω_1 expressed by **Eq.4**.

$$\omega_1 = \frac{1}{(h/R)_{max}} \int_0^{(h/R)_{max}} \left(\left(\frac{F}{E^* R^2} \right)_{exp} - \left(\frac{F}{E^* R^2} \right)_{model} \right)^2 d\left(\frac{h}{R} \right) \qquad \textbf{(Eq.4)}$$

The identification of the σ_y and n values which minimize ω_1 is led by a conjugate gradient algorithm. The identified material parameter values and the corresponding errors are presented in **Table 2**.

	σ_y *(MPa)*	Error (%)	n	Error (%)
MAT 1	197	- 1.5	0.000	/
MAT 2	209	+ 4.3	0.192	- 4.0
MAT 3	599	- 0.3	0.000	/
MAT 4	604	+ 0.6	0.199	- 0.5
MAT 5	1009	+ 1.0	0.000	/
MAT 6	1006	+ 0.5	0.200	0.0

Table 2. Material parameter values identified from ideal FEM indentation curves, minimising ω_1

Most identification errors are below 1 %, except for MAT 2 which shows errors of about 4 % on both σ_y and n values.

The identified stress-strain curves are compared to the stress-strain curves used for the FEM simulations in **Fig.4**.

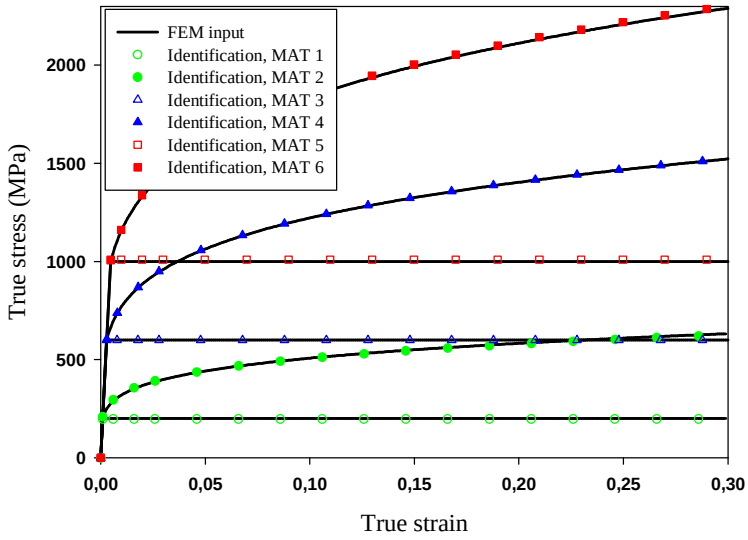

Fig.4. Comparison of the stress-strain curves identified from ideal FEM indentation curves to the stress-strain curves used in the FEM simulations, minimising ω_1

The identified stress-strain curves are in very good agreement with the stress-strain curves used in the FEM simulations, even for MAT 2, for which it can be suggested that compensation between material parameters provides a stress-strain curve which is very close to the one used in the FEM simulation.

This very good agreement validates the relevance of the model, its implementation, and the chosen identification procedure in the case of ideal experimental data. This allows the assessment in section **3** of the effect of an offset of the penetration depth on the identification results.

3. Effect of an offset of the penetration depth on the identification results

In section **2**, the experimental curve is supposed to be ideal, i.e. representative of the bulk material, presenting neither an offset of penetration depth nor effects on the slope of the *F-h* curve at low load values.

There is an interest in assessing the effect of an offset of penetration depth on the identification results. If one considers in first approximation that the offset is equal to half the distance between peak and valley in the case of a rough surface **[7]**, a dimensionless penetration depth offset h_{offset}/R=0.006 value can be assimilated, depending on the scale, to the indentation of a rectified surface presenting a R_a value of 1 µm by a sphere of radius 0.8 mm, as well as to the indentation of a mechanically polished surface presenting a R_a value of 0.2 µm by a sphere of radius 160 µm. An offset h_{offset}/R=0.006 is applied on all six FEM curves and the identification procedure presented in section **2** is applied, leading to the fitting of the curves obtained from the model to the offset FEM curves presented in **Fig.5**.

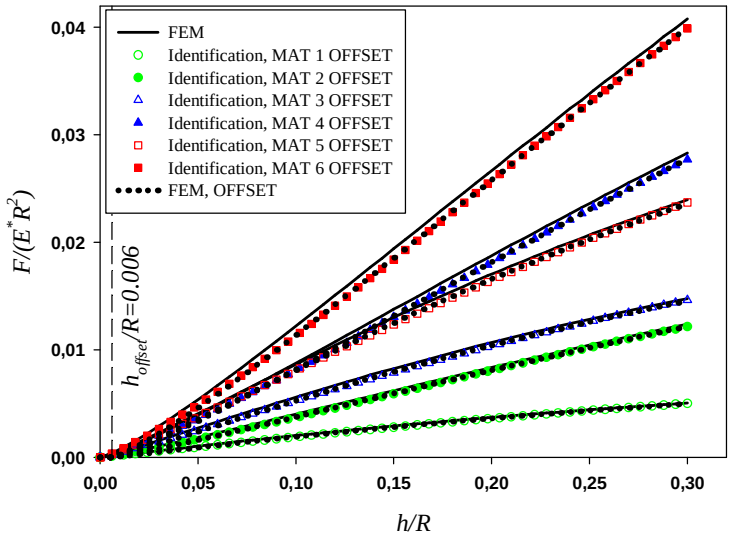

Fig.5. Fitting of the indentation curves obtained from the model to the offset FEM curves, minimising ω_1

The offset is more visible for curves presenting high slopes, i.e. for materials showing high mechanical parameter values. It can be expected that the effects on the identified material parameter values is also higher for curves presenting high slopes. The identified material parameter values are presented in **Table 3**.

	σ_y *(MPa)*	Error (%)	*n*	Error (%)
MAT 1	167	- 19.7	0.031	/
MAT 2	138	- 45.0	0.261	+ 30.5
MAT 3	479	- 25.1	0.055	/
MAT 4	408	- 47.1	0.281	+ 40.5
MAT 5	775	- 29.0	0.075	/
MAT 6	678	- 47.6	0.294	+ 47.0

Table 3. Material parameter values identified from offset FEM indentation curves, minimising ω_1

The resulting identification errors are significant, of an average value of 40 %. The errors are higher for materials showing high material parameter values. The identified stress-strain curves are compared to the stress-strain curves used in the FEM simulations in **Fig.6**.

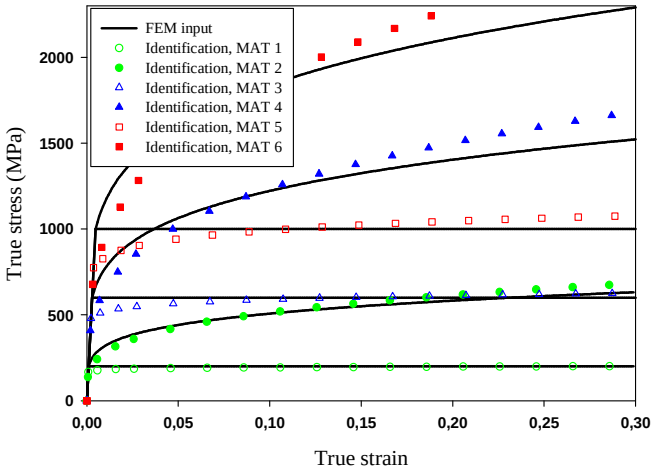

Fig.6. Comparison of the stress-strain curves identified from the offset FEM curves minimising ω_1 to the stress-strain curves used in the FEM simulations

The identified stress-strain curves are very different from the ones used in the simulations. The trend of the identification errors is consistent with the offset. Indeed, the offset FEM curve is closer to that of a material presenting a lower yield stress value and a higher hardening exponent value.

It is thus clear that a reliable identification of material properties through the use of models based on **Eq.2** using ω_1, i.e. a minimisation of load difference at known penetration depth values, cannot be carried out in the case of an offset of penetration depth due, for instance, to surface roughness or imperfect indenter tip geometry. In section **4**, an alternative approach is proposed to overcome this problem.

4. Proposition of a new approach independent of the offset of indentation depth

4.1. Proposition of a new cost functional

In section **3**, it is shown that a minimisation of the load difference at penetration depth values cannot provide a reliable identification of material properties in the case of an offset of the penetration depth measurement, when using identification models based on **Eq.2**. Therefore, there is an interest in developing an approach which is independent of the true penetration depth value. Mathematically, the offset on the penetration depth measurement creates a non zero intercept on the curve. A value which does not depend on this intercept is the slope of the curve, if plotted versus the indentation load. If the reverse analysis model defines the indentation load-depth relationship continuously over the penetration depth range, such as the model proposed by Ogasawara et al **[10]** and many others **[2, 4, 5, 8, 9, 11, 12]**, the derivative of the *F-h* function can be extracted. The slope of the indentation curve versus the indentation load is plotted for the indentation curves obtained from the FEM simulations, non offset and offset, and for the indentation curves obtained from the model, in **Fig.7**.

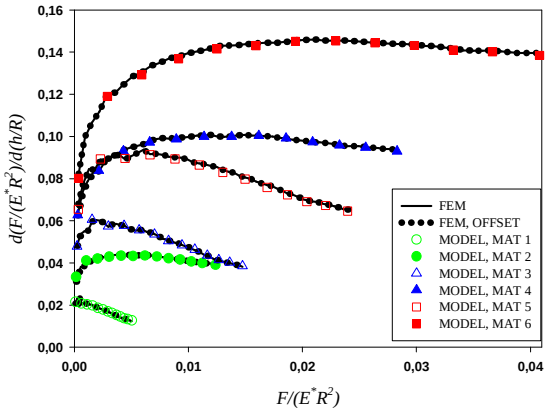

Fig.7. Slope of the indentation curve versus indentation load for the indentation curves obtained from the FEM simulations, non offset and offset, and for the indentation curves obtained from the model

The *F-h* curve obtained from the identification model obviously presents a zero intercept, i.e. zero load for zero penetration depth. Consequently, the relation between the indentation function given by the model and its derivative is unique, and the use of the derivative is as relevant as the use of the indentation function itself. Therefore, the proposition in this work is to use a new cost functional ω_2 which uses the slope of the indentation curve at indentation load values, such as expressed by **Eq.5**.

$$\omega_2 = \frac{1}{\left(F/E^*R^2\right)_{max}} \int_0^{\left(F/E^*R^2\right)_{max}} \left(\left(\partial\left(\frac{F}{E^*R^2}\right) \Big/ \partial\left(\frac{h}{R}\right) \right)_{exp} - \left(\partial\left(\frac{F}{E^*R^2}\right) \Big/ \partial\left(\frac{h}{R}\right) \right)_{model} \right)^2 d\left(\frac{F}{E^*R^2}\right)$$

(Eq.5)

The identification procedure presented in section **2** is applied minimising ω_2, and leads to the identified material parameter values presented in **Table 4**.

	σ_y *(MPa)*	Error (%)	*n*	Error (%)
MAT 1	199	- 0.5	0.000	/
MAT 2	198	- 1.0	0.203	+ 1.5
MAT 3	592	- 2.3	0.004	/
MAT 4	604	+ 0.6	0.199	- 0.5
MAT 5	983	- 1.9	0.009	/
MAT 6	1041	+ 3.8	0.189	- 5.5

Table 4. Material parameter values identified from offset FEM indentation curves, minimising ω_2

The range of errors of identification shows an average absolute value of 2%, which is slightly higher than the one obtained in section **2**, i.e. in the case of ideal FEM indentation curves minimising ω_1, nevertheless the identification results minimising ω_2 still show a very good agreement with the material parameter values used in the FEM simulations.

The identified stress-strain curves are compared to the stress-strain curves used in the FEM simulations in **Fig.8**.

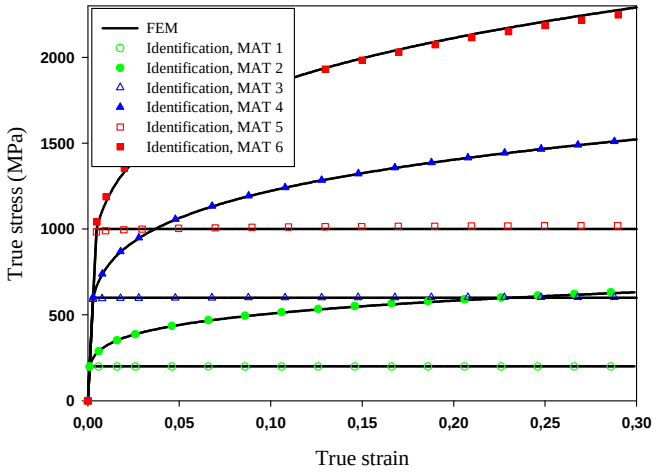

Fig.8. Comparison of the stress-strain identified from offset FEM indentation curves to the stress-strain curves used in the FEM simulations, minimising ω_2

The identified stress-strain curves show a very good agreement with the stress-strain curves used in the FEM simulations. As in the case of MAT 2 in the ideal identification case, the identified parameter values for MAT 6 seem to compensate one another and provide a good identification of the stress-strain curve. The overall good agreement validates the relevance of the use of the new cost functional ω_2 in the case of an offset of the penetration depth.

4.2. Neglecting the data at low load values

Independently of the offset of the penetration depth, there is an interest in proposing an approach which is little affected by the perturbation of the slope of the *F-h* curve at low load values. In the experimental application proposed in section **5**, the perturbation of the slope of the *F-h* curve reaches about 10% of the maximum load, therefore the identification procedure minimising ω_2 is applied neglecting the data corresponding to the lower 10 % load values. The identified material parameter values are presented in **Table 5**.

	σ_y *(MPa)*	Error (%)	*n*	Error (%)
MAT 1	200	0.0	0.000	/
MAT 2	213	+ 6.5	0.188	- 6.0
MAT 3	589	- 1.8	0.006	/
MAT 4	611	+ 1.8	0.196	- 2.0
MAT 5	984	- 1.6	0.009	/
MAT 6	1039	+ 3.9	0.190	- 5.0

Table 5. Material parameter values identified from offset FEM indentation curves, minimising ω_2 and neglecting the lower 10 % load values

The range of errors of identification is comparable with that obtained in the case of the use of all load values, except for MAT 2 for which it can once again be suggested that a compensation between material parameter values leads to opposite errors on both σ_y and *n* values. The identified stress-strain curves, which are not shown, are also in an agreement with the stress-strain curves used for the FEM simulations which is comparable to the agreement obtained in the case of the use of all load values (**Fig.8**).

The overall good agreement validates the relevance of the use of the new cost functional ω_2 in the case of an offset of the penetration depth as well as in the case of affected slope of the curve at low load values. The approach proposed in this work is applied to an experimental case in section **5**.

5. Experimental application

The experimental application proposed in this work focuses on the effect of imperfect indenter tip geometry on the indentation curve and on the identification results. The indented material is an AISI 1095 steel. The indenter is a rounded tip carved in bulk tungsten carbide, such as shown by the SEM visualization in **Fig.9.a**.

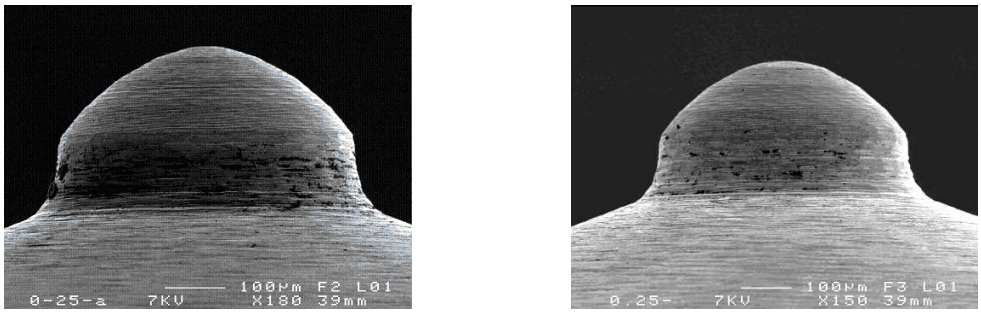

(a) **(b)**

Fig.9. Scanning Electron Microscopy (SEM) visualization of the indenter **(a)** before (x180) and **(b)** after (x150) tip alteration

In order to assess the influence of imperfect indenter tip geometry, the profile of the indenter is intentionally altered at the tip, such as shown in **Fig.9.b**. The profiles measured from the by SEM visualizations before and after alteration are compared in **Fig.10**.

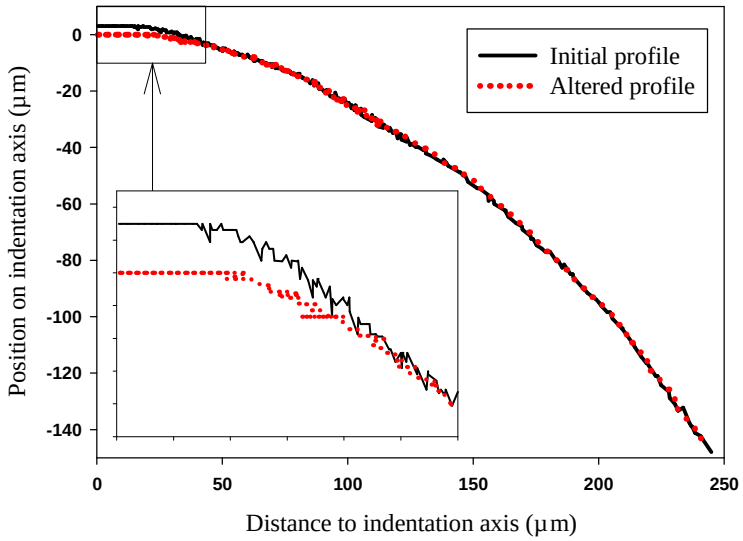

Fig.10. Indenter profiles before and after alteration of the tip

It is clear that only the geometry of the tip of the indenter is altered. Indentation tests are led up to a load of 200 N on a sample of AISI 1095 whose surface is mirror-like polished, before and after alteration of the indenter's profile. The indentation curves are presented in **Fig.11**.

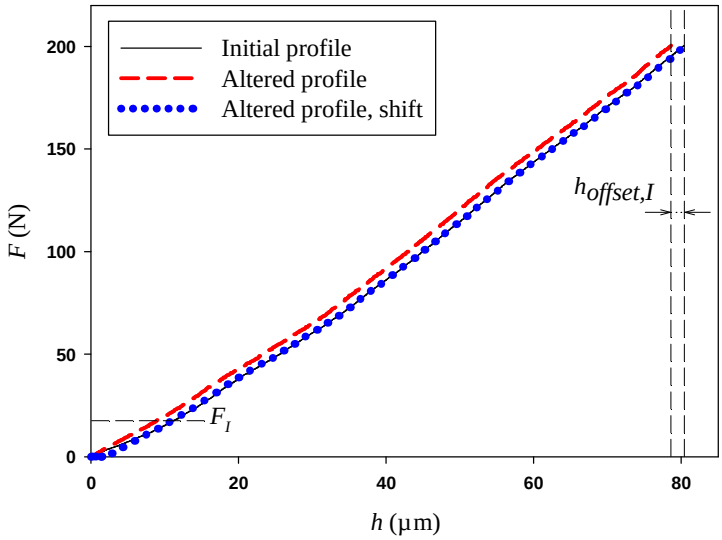

Fig.11. Experimental indentation curves before and after alteration of the indenter's profile

The indentation curves clearly show a difference of slope at low loads which corresponds to the alteration of the indenter's profile at its tip. After reaching a load of about 20 N (F_I), which represents 10% of the maximum load, the slopes of the curves are identical, as shown by the rightward shift of the curve obtained after alteration of the profile. This shift of about 2 µm is the penetration depth offset due to the imperfection of the indenter tip geometry, written $h_{offset,I}$ in **Fig.11**.

An in-house calibration procedure is available to take into account the real profile and the deformation of the indenter and obtain the results which would be obtained by a perfect rigid sphere, allowing the use of the model proposed by Ogasawara et al. However, this calibration procedure is defined for the initial profile of the indenter, thus the interest of this application is to determine if the approach proposed in this article can avoid the necessity to redefine the calibration procedure for the case of the altered tip profile.

Based on the data obtained by a tensile test and presented in a preceding article **[21]**, the Young modulus of the AISI 1095 steel is set to 210 GPa in the identification model. The identification procedure minimising ω_1 is applied to the indentation curves obtained before and after alteration of the tip profile over the whole indentation data. The identification

procedure minimising ω_2 is applied to the indentation curve obtained after deformation of the tip profile, using the values corresponding to load values higher than 20 N (F_1). The identified material parameter values are presented in **Table 6**.

	σ_y (MPa)	n
Initial profile, ω_1	211	0.218
Altered profile, ω_1	304	0.149
Altered profile, ω_2, F>20N	216	0.214

Table 6. Material parameter values identified by indentation with respect to the identification method for AISI 1095 steel

The material parameter values identified minimising ω_1 and the curve obtained after alteration of the tip profile are very different from those identified minimising ω_1 and the curve obtained before alteration of the tip profile. Indeed, the leftward relative position of the curve obtained after alteration of the tip profile corresponds to a material presenting a higher yield stress and a lower hardening coefficient. However, the material parameter values identified minimising ω_2 and the upper 90% of the curve obtained after alteration of the tip profile are very close to those obtained minimising ω_1 and the curve obtained before alteration of the tip profile. The identified stress-strain curves are compared to the stress-strain curve obtained by the tensile test in **Fig.12**.

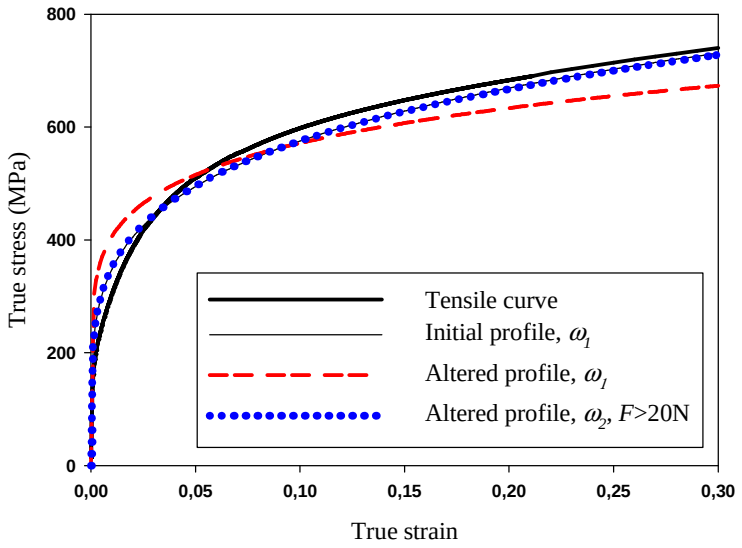

Fig.12. Comparison of the stress-strain curves obtained from identification by indentation to the stress-strain curve obtained from the tensile test

In the case of the initial profile, i.e. the ideal case, the identification of Hollomon law parameter values by instrumented indentation using the model proposed by Ogasawara et al and the cost functional ω_1 provides a very good evaluation of the stress-strain curve of the AISI 1095 steel obtained by the tensile test. The same exploitation of the data obtained with the altered tip profile provides a poor evaluation of the tensile curve due to the offset of the indentation curve. Indeed, the indentation curve is closer to that of a material presenting a higher yield stress value and a lower hardening exponent value. Nevertheless, the application of the approach proposed in this work provides an evaluation of the stress-strain curve of the AISI 1095 which is very close to the ideal case, i.e. a very good evaluation. In this application it is thus shown that even in the case of an altered indenter tip geometry, initial indenter geometry can be assumed if the approach proposed in this work is used. This approach can be used in the case of a crushed spherical indenter as well as in the case of a blunted conical indenter.

5. Conclusion

In this work, after validating the efficiency and the implementation of an identification model based on spherical indentation selected in indentation literature, the effect of an offset of penetration depth on identification results is assessed. In the case of the classical minimisation of the load difference at penetration depth values, results are much affected by a slight offset of penetration depth. An alternative exploitation of the identification model is proposed, based on the minimisation of the difference between the slopes of the *F-h* curves at indentation load values, leading to identification results which are comparable to the ones obtained by classical identification in the case of non offset indentation data. Moreover, the proposed alternative is little affected if the initial data in terms of load is neglected in the identification procedure, which is necessary in the case of significant effects of low scale artefacts on the slope of the *F-h* curve at low load values. Finally, an experimental case is presented, showing that the proposed alternative is relevant in the case of an indenter with an altered tip geometry.

In conclusion, the exploitation method of identification models in instrumented indentation proposed in this work is a reliable alternative to the determination of the effective zero point and redefinition of the *F-h* curve at low load values, and can be used to overcome the effects of many low scale artefacts such as sensor sensitivity, surface roughness, and

imperfect indenter tip geometry which are frequently encountered during micro and nanoindentation testing.

References

[1] S. Kucharski and Z. Mröz: Identification of plastic hardening parameters of metals from spherical indentation tests. Mater. Sci. Eng., A 318, 65 (2001).

[2] A. Nayebi, R. El Abdi, O. Bartier, G. Mauvoisin: New procedure to determine steel mechanical parameters from the spherical indentation technique. Mech. Mater. 34, 243 (2002).

[3] Y-P. Cao and J. Lu: A new method to extract the plastic properties of metal materials from an instrumented spherical indentation loading curve. Acta Mater. 52, 4023 (2004).

[4] H. Lee, J.H. Lee and G. M. Pharr: A numerical approach to spherical indentation techniques for material property evaluation. J. Mec. Phy. Sol. 53, 2037 (2005).

[5] M. Beghini, L. Bertini and V. Fontanari: Evaluation of the stress-strain curve of metallic materials by spherical indentation. Int. J. Sol. Struct. 43, 2441 (2006).

[6] M. Zhao, N. Ogasawara, N. Chiba and X-A. Chen: new approach to measure the elasticplastic properties of bulk materials using spherical indentation. Acta mater. 54, 23 (2006).

[7] Y. Cao, X. Qian and N. Huber: Spherical indentation into Elastoplastic materials : indentation-response based definitions of the representative strain. Mat. Sci. and Eng. A. 454, 1 (2007).

[8] J-M. Collin, G. Mauvoisin, O. Bartier, R. El Abdi and P. Pilvin: Experimental evaluation of the stress–strain curve by continuous indentation using different indenter shapes. Mat. Sci. and Eng A. 501, 140 (2009).

[9] J.-M. Collin, G. Mauvoisin and P. Pilvin: Materials characterization by instrumented indentation using two different approaches. Mat. Design. 31, 636 (2010).

[10] P. Jiang, T-H. Zhang, Y-H. Feng, and N-G. Liang: Determination of plastic properties by instrumented spherical indentation:Expanding cavity model and similarity solution approach. J. Mater.Res. 24, 1045 (2009).

[11] N. Ogasawara, N. Chiba and X. Chen: A simple framework of spherical indentation for measuring elastoplastic properties. Mech. Mater. 41, 1025 (2009).

[12] J.H. Lee, T. Kim, H. Lee : A study on robust indentation techniques to evaluate elastic-plastic properties of metals. Int. J. Sol. Struct. 47, 647 (2010).

[13] C. Ullner / Measurement 27 43 –51 (2000).

[14] C. Walter et al. / Surface & Coatings Technology 202, 1103–1107 (2007).

[15] A.C. Fischer-Cripps / Surface & Coatings Technology 200, 4153– 4165 (2006).

[16] T. Chudoba et al. / Surface and Coatings Technology 127, 9-17 (2000).

[17] S.R. Kalidindi, S. Pathak / Acta Materialia 56, 3523–3532 (2008).

[18] S. Pathak et al. / Scripta Materialia 60 (2009) 439–442

[19] J.-S. Park, et al., Surf. Coat. Technol. (2011)

[20] Hertz H: Uber die Berührung festischer Körper. J. Reine und Angew. Math. 92, 156 (1881).

[21] P. Brammer et al.: Influence of sample thickness and experimental device configuration on the spherical indentation of AISI 1095 steel. J. Mater. Res., Vol. 27, No. 1, Jan 14 (2012).